Ultrasonic sharp autofocusing with acoustic metasurface

Xue Jiang,[1,*] Yong Li,[2] Dean Ta,[1,†] and Weiqi Wang[1]
[1]*Department of Electronic Engineering, Fudan University, Shanghai 200433, China*
[2]*Institute of Acoustics, School of Physics Science and Engineering, Tongji University, Shanghai 200092, China*

(Received 28 May 2020; revised 22 July 2020; accepted 14 August 2020; published 25 August 2020)

Ultrasound focusing manifests itself as the accumulation of ultrasound energy on the target. It attracts extensive interest owing to its substantial advantage in engineering detection and biomedical science. However, the conventional focusing technique leads to the undesirable off-target influence in the nonfocusing region, hindering its application such as ultrasound surgery. Here we propose an ultrasound beam with idiosyncratic sharp autofocusing properties and implement it with the binary metasurface. The beam shows a sharp accumulation at the focus with an abrupt increase of intensity by three orders of magnitude while keeping the unintended region intact. The sharp autofocusing is realized by the controlled transverse self-acceleration and collapse of caustic at the focus in a nonlinear fashion. The intensity contrast, width, and position of the beam are highly tunable to realize the freewheeling focusing with high efficiency. Remarkably, the possibility to synthesize the abrupt autofocusing by the phase-only modulation is revealed. As an implementation, we demonstrate that the precise control of the sharp converging beam can be realized by an extremely simple metasurface with binary elements. The sharp autofocusing beams would open an avenue to realize the diverse ultrasound focusing with promising applications in medical ultrasound imaging, therapy, and nondestructive evaluation.

DOI: 10.1103/PhysRevB.102.064308

I. INTRODUCTION

Ultrasound beams are used for energy delivering on the target in numerous scenarios. Among the various technologies developed in ultrasound beam control, spatial ultrasound focusing has always been a subject of substantial significance which is widely deployed in versatile applications [1–14]. In nondestructive evaluation techniques, it is employed for inspecting materials with hidden flaws [13,14]. Focused ultrasound beams also play a key role in biomedical ultrasound imaging and therapy where the energy is converged to the targeted tissue [1–12]. Conventionally, the energy convergence of ultrasound beam is realized by curved focusing lens or active phased array, which gradually reshapes the wave front of the ultrasound beam with acoustic intensity smoothly accumulated until approaching the focal point. In this case, the energy of the ultrasound beam is delivered in a dispersed volume proportional to $\lambda^3(f/D)^4$, where λ is the wavelength, f is the focal length, and D is the transverse size of the beam on the initial source plane [15]. Therefore, the energy is spatially distributed in a relatively large volume, especially for low frequency and long focal length. For various applications, however, it is highly desirable to focus the ultrasound energy right onto the target in an abrupt manner, while maintaining the low intensity profile in other unintended areas. Particularly, the controlled sharp focusing contributes to biomedical ultrasound surgery where the beam should only impact the expected region while leaving any preceding tissue intact. It can be useful in particle trapping and manipulation with high precision and localization as well [16–18].

On the other hand, traditional ultrasound focusing is realized with the lens of curved shapes or phased array with the actively controlled elements [3,6]. The large size and sophisticated configurations of these techniques inevitably hinder their application in practice. Recent advances of acoustic metamaterial enable the unprecedent and effective sound focusing by controlling the phase delay in a planar structure with the substantially reduced thickness [19–32]. However, the spatial variations of the phase distribution for producing the focusing beam require a large amount of subwavelength unit cells with a complicated microstructure, which poses challenges to the fabrication process [19,27–29], especially for biomedical ultrasound whose typical wavelength is in the millimeter scale. It calls for a simpler and practically feasible configuration to realize the ultrasound focusing with compact metasurface, yet possessing the sharp autofocusing with negligible off-target influence to the nonfocusing region. The autofocusing beams have attracted wide interest in optics and acoustics [33–37], which render significant properties such as nondiffraction, self-healing, and multifocal.

In this work, we solve these difficulties by introducing a type of ultrasound beam with sharp autofocusing properties, and implementing it with a compact ultrasound metasurface consisting of only binary elements. The generated autofocusing ultrasound beam focuses in a nonlinear fashion, exhibiting the abrupt increase of acoustic intensity by three orders of magnitude at the focal point, while the intensity remains almost constant during the propagation. The comparison of the traditional acoustic focusing by the curved lens and complex metasurface, and the sharp autofocusing ultrasound beam in this work, is schematically illustrated in Fig 1. The

*xuejiang@fudan.edu.cn
†tda@fudan.edu.cn

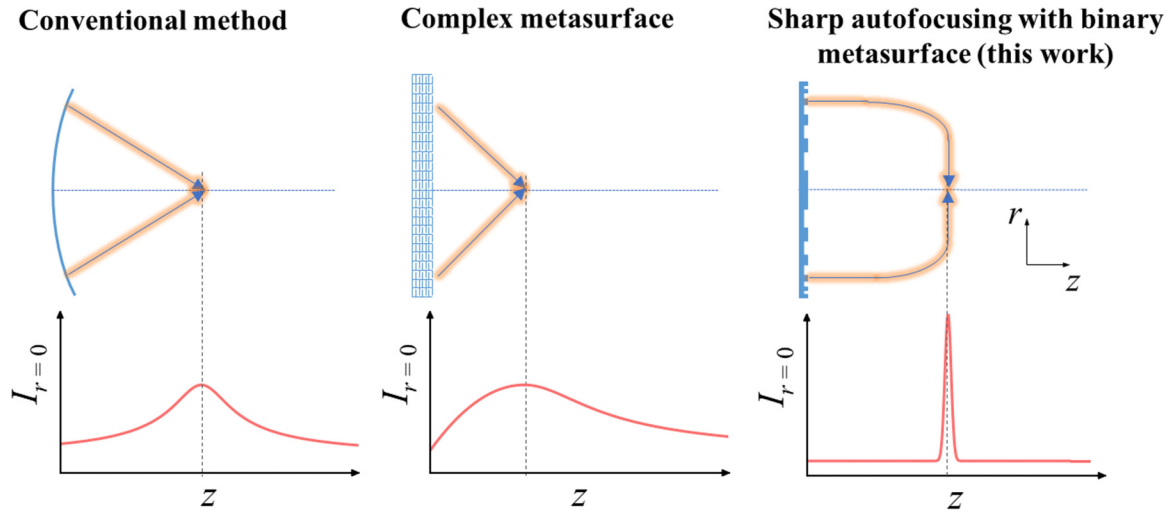

FIG. 1. Comparison of the traditional acoustic focusing by the curved lens (left), the complex metasurface (middle), and the sharp autofocusing ultrasound beam with the binary metasurface (right). Acoustic intensity in the traditional focusing along the axis is smoothly accumulated to the focal point. However, ultrasound intensity is abruptly increased in the sharp autofocusing beam while maintaining negligible in nonfocusing region.

ultrasharp autofocusing comes from the unique transverse self-acceleration of the proposed beam and resultant accelerating energy flux near the focal plane. The intensity, focal position, and width of the autofocusing beam are highly tunable, showing the capability and flexibility to achieve discretionary focusing while ensuring high intensity contrast, precise focal position, high efficiency, and subdiffraction-limit resolution. In order to facilitate the implementation of this beam, we further explore the possibility to synthesize the abrupt autofocusing only by manipulating the phase distribution. Remarkably, the sharp focusing and precise control of the beam is realized with a simple planar surface with binary elements. With sudden convergence of sound energy by three orders of magnitude and extreme simplicity in metasurface realization, as well as the flexible tunability, the proposed sharp autofocusing ultrasound beams possess fascinating prospects in practical applications such as biomedical ultrasound surgery, nondestructive evaluation, and particle manipulation.

II. THEORETICAL DESIGN

We start by considering the propagation of axisymmetric beams in cylindrical coordinates depending only on r and z, as illustrated in Fig. 1. The sharp autofocusing ultrasound beam is proposed based on the circular Airy distribution of pressure on the initial launch plane $p(r, z = 0) = p_0(r)$, which is radially symmetric and described by [38,39]

$$p_0(r) = \mathrm{Ai}\left(\frac{r_0 - r}{w}\right) \exp\left(\alpha \frac{r_0 - r}{w}\right), \tag{1}$$

where $\mathrm{Ai}(\cdot)$ denotes the Airy function, r_0 is the initial radius of the primary ring, and w is a scale factor. Here α is an exponential decay factor to ensure that the wave conveys finite energy, yet it is typically small to keep the behavior of the wave approximating an ideal diffraction-free Airy wave packet in general. It has been proved that the Airy function is the nondiffraction solution of the time-harmonic paraxial wave equation, and the resultant sound beam follows the parabolic trajectory. The profile of pressure p_0 on the initial plane ($z = 0$) is shown in Fig. 2(a), with the parameters of $r_0 = 4.6\lambda$, $w = 1.1\lambda$, and $\alpha = 0.05$, where λ is the wavelength of the ultrasound beam. From Eq. (1) and Fig. 2(a), it is readily seen that for $r < r_0$, the ultrasound beam decays exponentially, whereas the oscillations of the Airy tails slowly decay outside this region. The fast Fourier transform (FFT) amplitude of p_0 as a function of the radial spectral component k is depicted in Fig. 2(b), where the FFT amplitude oscillates between positive and negative values with a decreasing envelope. The power carried by the circular Airy beam is given by

$$P = 2\pi \int_0^\infty |p_0(r)|^2 r dr = \sqrt{\frac{\pi}{2\alpha}}\, e^{2\alpha^3/3}\left(\frac{r_0}{w} + \frac{1 - 4\alpha^3}{4\alpha}\right). \tag{2}$$

We carried out the numerical simulations to investigate the sharp autofocusing characteristics of the proposed ultrasound beam. Throughout this paper, the numerical simulations are conducted by the finite element method based on commercial software COMSOL Multiphysics. The background medium is water, with the mass density and ultrasound speed being $1000\,\mathrm{kg/m^3}$ and $1500\,\mathrm{m/s}$, respectively. Without losing generality, we consider the ultrasound of frequency 500 kHz and wavelength $\lambda = 3$ mm. The input pressure p_0 on the initial launch plane ($z = 0$) has the form as in Eq. (1). The intensity contrast G, defined as the ratio of the ultrasound intensity to the average intensity on the initial source plane, is introduced to quantitatively evaluate the intensity enhancement and energy confinement. The distribution of the intensity contrast G of the generated ultrasound beam is illustrated in Fig. 2(c), where the ultrasharp focusing behavior is observed. Despite the intensity oscillation, the maximum intensity for every z remains almost a negligible value. On the contrary, at the focal

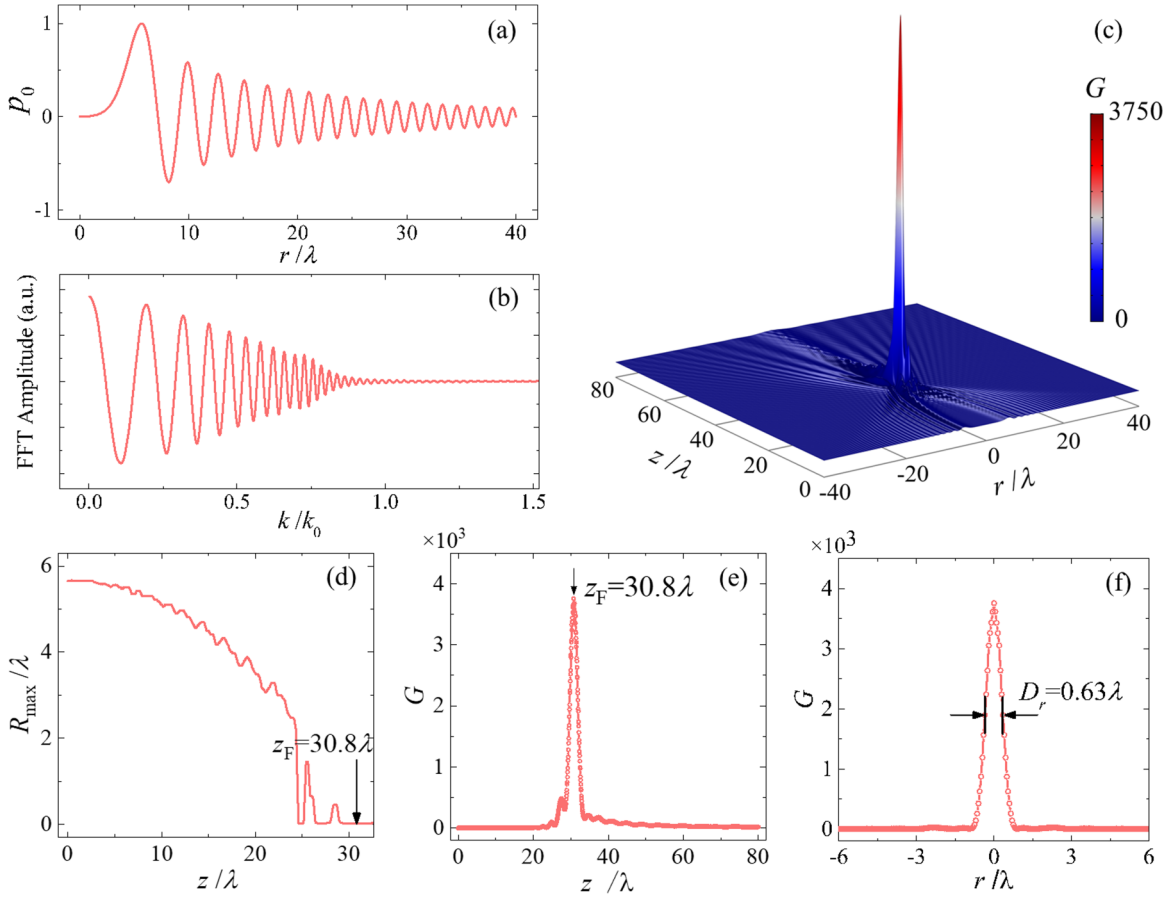

FIG. 2. Evolution of the sharp autofocusing ultrasound beam for $r_0 = 4.6\lambda$, $w = 1.1\lambda$, and $\alpha = 0.05$. (a) The profile of the normalized ultrasound pressure p_0 on the initial source plane ($z = 0$). (b) The FFT amplitude of the pressure p_0 on the initial source plan. (c) Intensity contrast G evolution of the autofocusing ultrasound beam. Ultrasound beam emitted from the source plane automatically converge to a small focal point at the designated position, resulting in the drastic enhancement of ultrasound energy. The intensity contrast G is defined as the ratio of the ultrasound intensity to the average intensity on the initial source plane ($z = 0$). (d) Radius coordinate r of the highest intensity of the beam during propagation. The maximum intensity converges in a nonlinear fashion, enabling the abrupt autofocusing. Intensity contrast G of the autofocusing ultrasound beam (e) along the propagating direction ($r = 0$) and (f) on the focal plane ($z_F = 30.8\lambda$) and FWHM (D_r) is 0.63λ.

point $z_F = 30.8\lambda$, a large inward transverse velocity is attained and the energy rushes in an accelerated fashion toward the focal point, leading to a rapid increase of the ultrasound intensity. We define the radius of the ultrasound Airy ring $R_{max}(z)$ as the radial position of the maximum intensity for every distance z. It describes the caustic surface evolution of the autofocusing beam [40,41], as displayed in Fig. 2(d). It shows that the caustic possesses an increased transverse velocity and bends toward the axis with acceleration, which abruptly collapses at the focal point. For a better view of the performance of the autofocusing ultrasound beam, we give the distributions of the intensity contrast G near the focal point along the axis ($r = 0$) and on the focal plane ($z_F = 30.8\lambda$) in Figs. 2(e) and 2(f), respectively. Significantly, the three orders of magnitude abrupt increase of the intensity contrast G is clearly observed in Fig. 2(e), which reaches 3750 at the focal point. Moreover, the full width at half maximum (FWHM) of the sharp autofocusing beam D_r is only 0.63λ, which unambiguously evidences the effective focusing property of the proposed ultrasound beam.

III. TUNABILITY OF THE SHARP AUTOFOCUSING PROPERTIES

To realize the on-demand autofocusing, we further analyze the tunability of the discussed ultrasound beam by controlling the input pressure p_0 on the initial source plane. In order to maintain the finite energy of the ultrasound beam and facilitate the practical implementation, the decay factor $\alpha = 0.05$ is set to be constant, so the initial source plane and ultrasound beam can be controlled by manipulating the initial radius r_0 and the scale factor w. For every set of parameters (r_0, w), we calculate the maximum intensity contrast G_{max} in the spatial field, and the profile of G_{max} as functions of r_0 and w is displayed in Fig. 3(a). The white contour in Fig. 3(a) indicates the parameter space where the maximum contrast G_{max} is larger than 1000 ($\log_{10}(G_{max}) > 3$). It demonstrates that a relatively large contrast G_{max} can be obtained in a wide range of parameter combinations by appropriately choosing the parameters, and the intensity contrast peak can be maximized to be around 4000. Much higher values of G_{max} can be

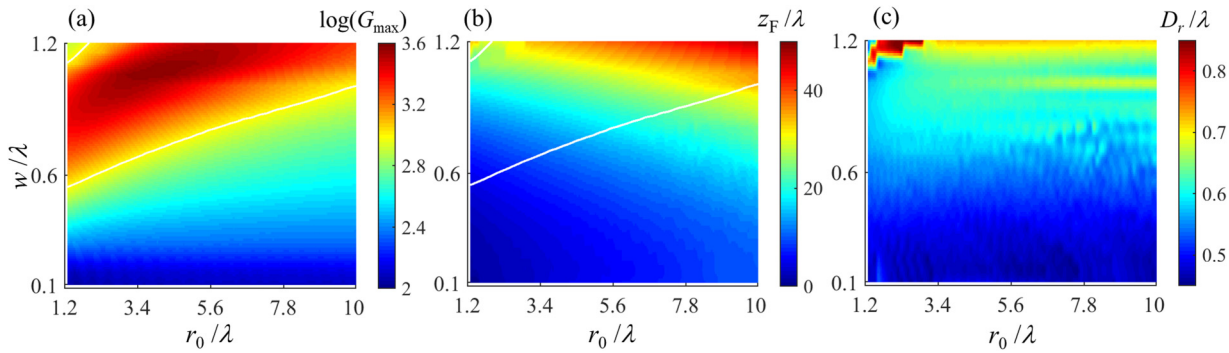

FIG. 3. Tunable intensity contrast and focal position of the sharp autofocusing beam. (a) The intensity contrast G, (b) the focal length z_F, and (c) the FWHM D_r as functions of the initial radius r_0 and scaling factor w in Eq. (1). The white contours in (a) and (b) indicate the parameter space where G_{max} is larger than 1000. The focal position can be freely controlled from 0.32λ to 47.8λ. The FWHM D_r over the whole considered parameter range is smaller than 0.85λ.

accessed by further suppressing the diffraction by decreasing the decay factor α. Meanwhile, the corresponding focal length z_F and the FWHM D_r of the sharp autofocusing beam are illustrated in Figs. 3(b) and 3(c). Remarkably, the energy of the ultrasound beam can be freely focused to arbitrary positions ranging from the very near field to far field by adjusting the parameters of the initial pressure covering the focal length z_F from 0.32λ to 47.8λ [Fig. 3(c)]. Moreover, the focal length z_F within the white contour ($G_{max} > 1000$) ranges from 4.7λ to 47.8λ, proving the high tunability of the on-demand autofocusing while maintaining the desired sharp energy increase. It is noteworthy that over the whole considered parameter space, the FWHM remains smaller than 0.85λ. In a certain parameter space, it approaches 0.45λ which is well beyond the diffraction limit, as a result of the interference and diffraction of the Airy rings in the near-field region [28,42]. The numerical results convincingly evidence the flexibility of the proposed sharp autofocusing ultrasound beam to generate the discretionary focusing while ensuring high intensity contrast, precise position, high efficiency, and subdiffraction-limit resolution.

IV. REALIZATION WITH PHASE-ONLY MODULATION

In principle, the amplitude and phase of ultrasound pressure on the initial source plane should simultaneously satisfy the requirement for generating the sharp autofocusing beam. Yet it is challenging in experiment and industry to independently manipulate these two degrees of freedom, either by the active phased array based on the sophisticated electronic control or with the passive metascreen consisting of numerous microstructures, especially for the large input source where large amounts of elements are needed. Alternatively, the control of the pressure phase has been proved to be achievable by active phased array or various passive metasurface for airborne sound. Therefore, it is necessary to investigate the possibility to synthesize the sharp autofocusing only with the phase modulation, which would greatly facilitate the realization in practical applications. Hereinafter, we introduce a source plane with the modified initial pressure p_1, which inherits the phase profile of the ideal initial pressure p_0 but with unitary amplitude. The comparison of the amplitude (blue lines) and phase (red lines) between p_0 (upper) and p_1 (lower) is illustrated in Fig. 4(a), with the same parameters (α, r_0, w) as in Fig. 2. The propagation dynamics of the autofocusing ultrasound beam are demonstrated in Fig. 4(b). Compared with the results in the ideal case, the reduced requirement of the initial amplitude distribution moderately weakens the interference and diffraction of the Airy rings in the near field. It leads to a slight difference in the intensity oscillation feature. However, the modification with the phase-only modulation has nearly no influence on the sharp autofocusing properties. It is clear that the ultrasound energy flux abruptly concentrates at the focal point, giving rise to the rapid and tremendous increase of the intensity. A maximum intensity contrast G of 3736 is obtained which is quantitatively similar to the idea case (3750). The profiles of G along the axis ($r = 0$) and on the focal plane ($z = z_F$) are shown in Figs. 4(c) and 4(d), respectively. The ultrasound intensity is converged to the identical focal position $z_F = 30.8\lambda$ as in the ideal case in Fig. 2(e), and the FWHM keeps the same as $D_r = 0.63\lambda$. These results prove that the proposed sharp autofocusing ultrasound beam can be conveniently synthesized with the phase-only modulation, which provides an effective methodology to implement it in practice.

V. IMPLEMENTATION WITH BINARY ULTRASOUND METASURFACE

To achieve the application of autofocusing in compact devices, we consider the implementation of the sharp autofocusing ultrasound beam with the passive ultrasound metasurface. Particularly, we employed a simple planar surface decorated with the grooves of $\lambda/4$ depth, which provides the binary phase delay 0 and π of the reflected ultrasound wave. It has been reported that the metasurface with the phase-only modulation can generate the Airy beam maintaining the key features such as the self-acceleration, nondiffraction, and self-healing [36,43], which enables the implementation of the sharp autofocusing in our work. The schematic plot of the ultrasound metasurface is illustrated in Fig. 5(a), where the normally incident sound wave will acquire phase delay of 0 or π after being reflected by the metasurface, which effectively satisfies the requirement of the phase profile in

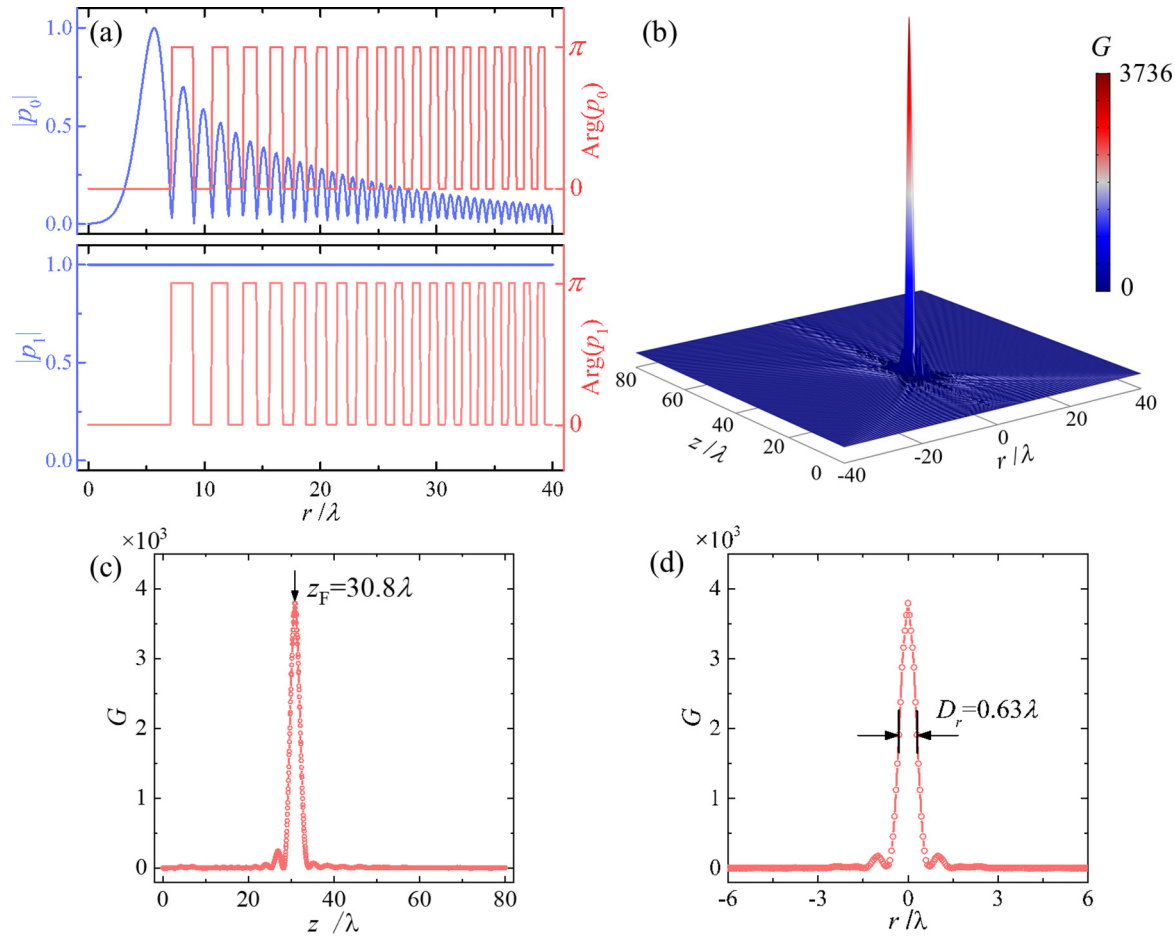

FIG. 4. Autofocusing behavior of the ultrasound beam generated by phase modulation. (a) Comparison of the amplitude and phase profiles between the ideal pressure p_0 (upper panel) and modified pressure p_1 (lower panel). The p_1 maintains the phase of p_0 while modified with the unitary amplitude. (b) Intensity evolution of the autofocusing ultrasound beam generated with the phase modulation. Autofocusing behavior remains similar. (c),(d) Intensity contrast profiles along the axis ($r = 0$) and on the focal plane ($z_F = 30.8\lambda$). The intensity converges at the identical focal position as in Fig. 2, and the FWHM D_r keeps the same $D_r = 0.63\lambda$.

Fig. 4(b). Here, the operating frequency is 500 kHz, and the depth of the grooves is only 0.75 mm. As a result, the reflected ultrasound beam by the binary metasurface undergoes the sharp autofocusing and tremendous energy accumulation at the targeted position, while the intensity in other unintended areas keeps as negligible values. As expected, the ultrasound energy is exactly converged at the identical focal point as in Figs. 2 and 4, and the FWHM nearly remains the same, while the near field differs from Fig. 2 arising from the absence of the amplitude manipulation. Benefiting from the simplicity and the ultrathin thickness, the binary metasurface provides an easy and lower-cost method to generate the proposed sharp autofocusing ultrasound beam in compact practical devices.

VI. DISCUSSION

In conclusion, we introduce the sharp autofocusing ultrasound beam endowed with the abrupt increase of the intensity by three orders of magnitude at the focal point while maintaining an almost constant intensity in unintended areas. The sharp autofocusing feature of the ultrasound beam stems from the transverse self-acceleration and nonlinear collapse of the caustic of the beam, giving rise to the accelerated accumulation of the internal energy flux at the target focal position. The focus intensity and position are found highly tunable, which unveils the flexibility to achieve discretionary focusing while ensuring the high intensity contrast, precise position, high efficiency, and subdiffraction-limit resolution. We further demonstrate the implementation of the autofocusing beam with a compact planar ultrasound metasurface consisting of only binary elements. The working frequency of the ultrasound metasurface presented here (500 kHz) is a typical frequency used in biomedical ultrasound, and the smallest geometric scale in the metasurface is 0.75 mm, which can be expediently fabricated with the current processing technologies such as three-dimensional printing and fine machining technologies, facilitating the experimental realization and promoting the application in practice. Remarkably, the performance of the proposed sharp autofocusing ultrasound beam is not limited by this specific metasurface. Any other metastructure with the phase control capability is suitable for the implementation, due to the reduced requirement of the beam modulation revealed by our study. The working frequency can be further tuned by scaling the metastructure

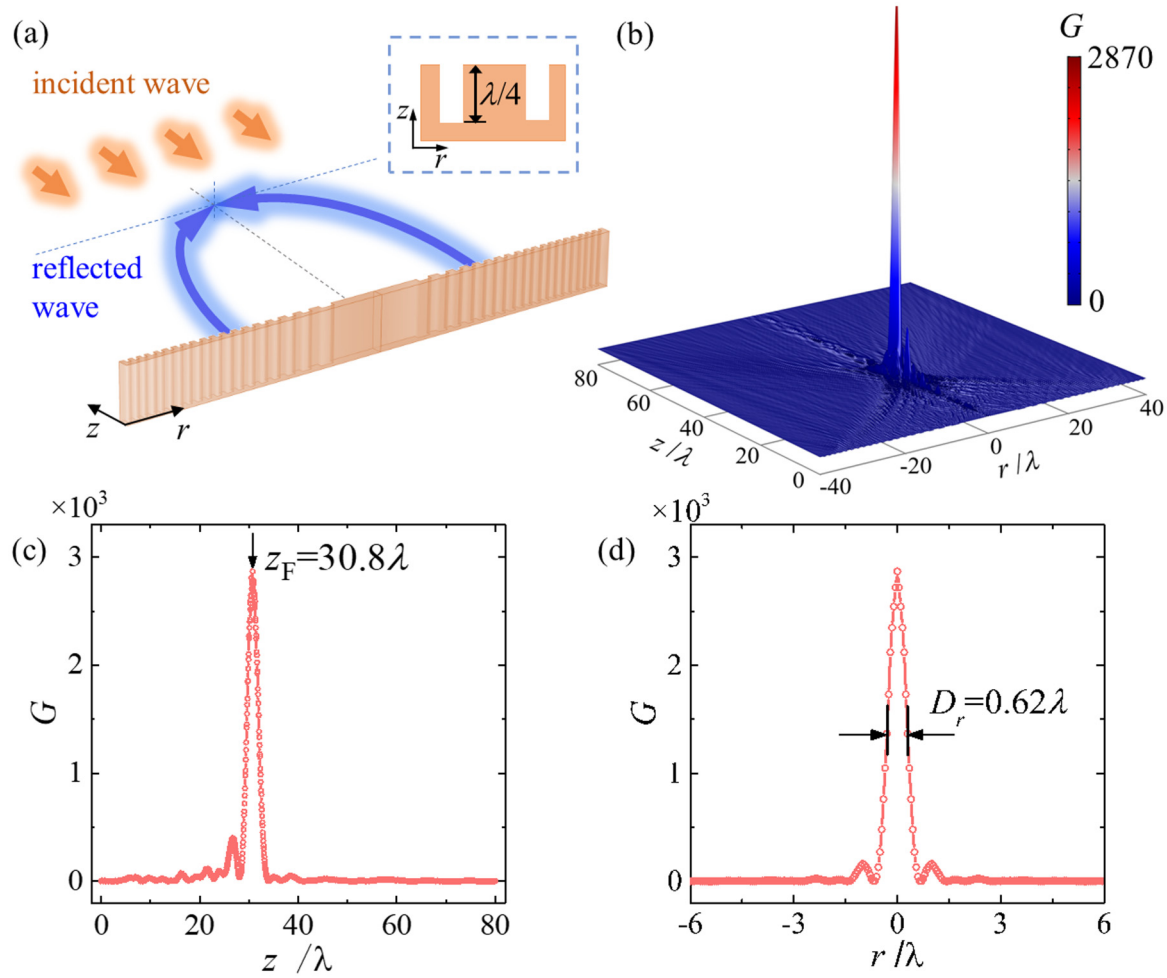

FIG. 5. Autofocusing ultrasound beam generated by the binary metasurface. (a) Schematic plot of the ultrasound metasurface consisting of grooves with the depth $\lambda/4$, providing the binary (0 and π) phase modulations of the reflected wave. The inset shows enlarged view of the metasurface. (b) Intensity evolution of the autofocusing beam generated with the metasurface. (c) Intensity contrast G along the axis, with the sharp increase of energy at the focal point $z_F = 30.8\lambda$. (d) Intensity contrast G on the focal plane as a function of r. The FWHM is $D_r = 0.62\lambda$.

or by employing other types of metasurface. We anticipate the simplicity in realization of the ultrasharp autofocusing ultrasound beam with abrupt convergence of sound energy. The proposed tunable autofocusing ultrasound beam may establish a platform for arbitrary beam control and shed light on the versatile applications in biomedical ultrasonography, nondestructive evaluation, and particle manipulation.

ACKNOWLEDGMENT

This work is supported by National Natural Science Foundation of China (Grants No. 11904055, No. 11525416, and No. 11827808), the Young Elite Scientists Sponsorship Program by CAST, Shanghai Committee of Science and Technology (Grant No. 20ZR1404200), and Program of Shanghai Academic Research Leader (Grant No.19XD1400500).

[1] W. Legon, T. F. Sato, A. Opitz, J. Mueller, A. Barbour, A. Williams, and W. J. Tyler, Transcranial focused ultrasound modulates the activity of primary somatosensory cortex in humans, Nat. Neurosci. **17**, 322 (2014).

[2] C. Mougenot, M. O. Köhler, J. Enholm, B. Quesson, and C. Moonen, Quantification of near-field heating during volumetric MR-HIFU ablation, Med. Phys. **38**, 272 (2011).

[3] J. W. Hand, A. Shaw, N. Sadhoo, S. Rajagopal, R. J. Dickinson, and L. R. Gavrilov, A random phased array device for delivery of high intensity focused ultrasound, Phys. Med. Biol. **54**, 5675 (2009).

[4] G. T. Clement and K. Hynynen, A non-invasive method for focusing ultrasound through the human skull, Phys. Med. Biol. **47**, 1219 (2002).

[5] R. Seip, P. VanBaren, and E. S. Ebbini, Dynamic focusing in ultrasound hyperthermia treatments using implantable hydrophone arrays, IEEE Trans. Sonics Ultrason. **41**, 706 (1994).

[6] L. R. Gavrilov and J. W. Hand, A theoretical assessment of the relative performance of spherical phased arrays for ultrasound surgery, IEEE Trans. Sonics Ultrason. **47**, 125 (2000).

[7] W. J. Elias, N. Lipsman, W. G. Ondo, P. Ghanouni, Y. G. Kim, W. Lee, M. Schwartz, K. Hynynen, A. M. Lozano, B. B. Shah, D. Huss, R. F. Dallapiazza, R. Gwinn, J. Witt, S. Ro, H. M. Eisenberg, P. S. Fishman, D. Gandhi, C. H. Halpern, R. Chuang *et al.*, A randomized trial of focused ultrasound thalamotomy for essential tremor, New England J. Medicine **375**, 730 (2016).

[8] F. Wu, W.-Z. Chen, J. Bai, J.-Z. Zou, Z.-L. Wang, H. Zhu, and Z.-B. Wang, Pathological changes in human malignant carcinoma treated with high-intensity focused ultrasound, Ultrasound Med. Biol. **27**, 1099 (2001).

[9] P.-Y. Chen, H.-L. Liu, M.-Y. Hua, H.-W. Yang, C.-Y. Huang, P.-C. Chu, L.-A. Lyu, I.-C. Tseng, L.-Y. Feng, H.-C. Tsai, S.-M. Chen, Y.-J. Lu, J.-J. Wang, T.-C. Yen, Y.-H. Ma, T. Wu, J.-P. Chen, J.-I. Chuang, J.-W. Shin, C. Hsueh, and K.-C. Wei, Novel magnetic/ultrasound focusing system enhances nanoparticle drug delivery for glioma treatment, Neuro-oncol. **12**, 1050 (2010).

[10] H. Kim, A. Chiu, S. D. Lee, K. Fischer, and S.-S. Yoo, Focused ultrasound-mediated non-invasive brain stimulation: examination of sonication parameters, Brain Stimulation **7**, 748 (2014).

[11] W. Lee, H.-C. Kim, Y. Jung, Y. A. Chung, I.-U. Song, J.-H. Lee, and S.-S. Yoo, Transcranial focused ultrasound stimulation of human primary visual cortex, Sci. Rep. **6**, 34026 (2016).

[12] R. L. King, J. R. Brown, and K. B. Pauly, Localization of ultrasound-induced in vivo neurostimulation in the mouse model, Ultrasound Med. Biol. **40**, 1512 (2014).

[13] S. Chatillon, G. Cattiaux, M. Serre, and O. Roy, Ultrasonic non-destructive testing of pieces of complex geometry with a flexible phased array transducer, Ultrasonics **38**, 131 (2000).

[14] S. W. Shin, A. R. Qureshi, J.-Y. Lee, and C. B. Yun, Piezoelectric sensor based nondestructive active monitoring of strength gain in concrete, Smart Mater. Struct. **17**, 055002 (2008).

[15] D. G. Papazoglou, N. K. Efremidis, D. N. Christodoulides, and S. Tzortzakis, Observation of abruptly autofocusing waves, Opt. Lett. **36**, 1842 (2011).

[16] J. Lee, S.-Y. Teh, A. Lee, H. H. Kim, C. Lee, and K. K. Shung, Single beam acoustic trapping, Appl. Phys. Lett. **95**, 073701 (2009).

[17] D. Baresch, J.-L. Thomas, and R. Marchiano, Observation of a Single-Beam Gradient Force Acoustical Trap for Elastic Particles: Acoustical Tweezers, Phys. Rev. Lett. **116**, 024301 (2016).

[18] M. Baudoin, J.-C. Gerbedoen, A. Riaud, O. B. Matar, N. Smagin, and J.-L. Thomas, Folding a focalized acoustical vortex on a flat holographic transducer: Miniaturized selective acoustical tweezers, Sci. Adv. **5**, eaav1967 (2019).

[19] S. Zhang, L. Yin, and N. Fang, Focusing Ultrasound with an Acoustic Metamaterial Network, Phys. Rev. Lett. **102**, 194301 (2009).

[20] J. Li, L. Fok, X. Yin, G. Bartal, and X. Zhang, Experimental demonstration of an acoustic magnifying hyperlens, Nat. Mater. **8**, 931 (2009).

[21] N. Kaina, F. Lemoult, M. Fink, and G. Lerosey, Negative refractive index and acoustic superlens from multiple scattering in single negative metamaterials, Nature (London) **525**, 77 (2015).

[22] Y. Li, X. Jiang, R. Li, B. Liang, X. Zou, L. Yin, and J. Cheng, Experimental Realization of Full Control of Reflected Waves with Subwavelength Acoustic Metasurfaces, Phys. Rev. Appl. **2**, 064002 (2014).

[23] Y. Shen, X. Zhu, F. Cai, T. Ma, F. Li, X. Xia, Y. Li, C. Wang, and H. Zheng, Active Acoustic Metasurface: Complete Elimination of Grating Lobes for High-Quality Ultrasound Focusing and Controllable Steering, Phys. Rev. Appl. **11**, 034009 (2019).

[24] C. Rubio, J. M. Fuster, S. Castiñeira-Ibáñez, A. Uris, F. Belmar, and P. Candelas, Pinhole zone plate lens for ultrasound focusing, Sensors **17**, 1690 (2017).

[25] S. Qi, Y. Li, and B. Assouar, Acoustic Focusing and Energy Confinement Based on Multilateral Metasurfaces, Phys. Rev. Appl. **7**, 054006 (2017).

[26] J. Zhao, H. Ye, K. Huang, Z. N. Chen, B. Li, and C.-W. Qiu, Manipulation of acoustic focusing with an active and configurable planar metasurface transducer, Sci. Rep. **4**, 06257 (2014).

[27] Y. Li, B. Liang, X. Tao, X. Zhu, X. Zou, and J. Cheng, Acoustic focusing by coiling up space, Appl. Phys. Lett. **101**, 233508 (2012).

[28] X. Jiang, B. Liang, J. Yang, J. Yang, and J. Cheng, Acoustic planar antireflective focusing lens with sub-diffraction-limit resolution based on metamaterials, J. Appl. Phys. **123**, 091717 (2018).

[29] Y.-X. Shen, Y.-G. Peng, F. Cai, K. Huang, D.-G. Zhao, C.-W. Qiu, H. Zheng, and X.-F. Zhu, Ultrasonic super-oscillation wave-packets with an acoustic meta-lens, Nat. Commun. **10**, 3411 (2019).

[30] W. Wang, Y. Xie, A. Konneker, B.-I. Popa, and S. A. Cummer, Design and demonstration of broadband thin planar diffractive acoustic lenses, Appl. Phys. Lett. **105**, 101904 (2014).

[31] P. Peng, B. Xiao, and Y. Wu, Flat acoustic lens by acoustic grating with curled slits, Phys. Lett. A **378**, 3389 (2014).

[32] J. Chen, J. Rao, D. Lisevych, and Z. Fan, Broadband ultrasonic focusing in water with an ultra-compact metasurface lens, Appl. Phys. Lett. **114**, 104101 (2019).

[33] M. M. Shanei, M. Hashemi, and C. J. Zapata-Rodríguez, Unconventional, efficient and flexible bifocal lens design by metalens and AFA beam combination, J. Opt. **21**, 055101 (2019).

[34] M. Hashemi, Dielectric metalenses with off-axis and multi-focal spots based on converging Airy beams with different initial velocities or accelerations, J. Phys. D: Appl. Phys. **53**, 175105 (2020).

[35] Q. Fan, D. Wang, P. Huo, Z. Zhang, Y. Liang, and T. Xu, Autofocusing Airy beams generated by all-dielectric metasurface for visible light, Opt. Express **25**, 9285 (2017).

[36] H. Gao, Z. Gu, B. Liang, X. Zou, J. Yang, J. Yang, and J. Cheng, Acoustic focusing by symmetrical self-bending beams with phase modulations, Appl. Phys. Lett. **108**, 073501 (2016).

[37] D.-C. Chen, X.-F. Zhu, Q. Wei, D.-J. Wu, and X.-J. Liu, Broadband acoustic focusing by Airy-like beams based on acoustic metasurfaces, J. Appl. Phys. **123**, 044503 (2018).

[38] U. Bar-Ziv, A. Postan, and M. Segev, Observation of shape-preserving accelerating underwater acoustic beams, Phys. Rev. B **92**, 100301 (2015).

[39] N. K. Efremidis and D. N. Christodoulides, Abruptly autofocusing waves, Opt. Lett. **35**, 4045 (2010).

[40] E. Greenfield, M. Segev, W. Walasik, and O. Raz, Accelerating Light Beams along Arbitrary Convex Trajectories, Phys. Rev. Lett. **106**, 213902 (2011).

[41] P. Zhang, T. Li, J. Zhu, X. Zhu, S. Yang, Y. Wang, X. Yin, and X. Zhang, Generation of acoustic self-bending and bottle beams by phase engineering, Nat. Commun. **5**, 4316 (2014).

[42] K. Huang, H. Ye, J. Teng, S. P. Yeo, B. Luk'yanchuk, and C.-W. Qiu, Optimization-free superoscillatory lens using phase and amplitude masks, Laser & Photon. Rev. **8**, 152 (2014).

[43] Q. Lu, S. Gao, Y. Ni, J. Wu, and Y. Qiao, Generation of Airy beams using a phase-only Fresnel holographic lens, Optoelectron. Lett. **13**, 197 (2017).